Geological record and reconstruction of the late Pliocene impact of the Eltanin asteroid in the Southern Ocean

R. Gersonde*, F. T. Kyte†, U. Bleil‡, B. Diekmann*, J. A. Flores§, K. Gohl‖, G. Grahl‡, R. Hagen¶, G. Kuhn*, F. J. Sierro§, D. Völker‡, A. Abelmann* & J. A. Bostwick†

* *Alfred Wegener Institute for Polar and Marine Research, Postbox 120161, D-27515 Bremerhaven, Germany*
† *Institute of Geophysics and Planetary Physics, UCLA, Los Angeles, California 90095, USA*
‡ *Fachbereich Geowissenschaften, University Bremen, Postbox 330440, D-28334 Bremen, Germany*
§ *Department of Geology, University of Salamanca, S-37008 Salamanca, Spain*
‖ *Macquarie University, School of Earth Sciences, Sydney NSW 2109, Australia*
¶ *Naval Research Lab.-Code 7420, 4555 Overlook Ave., SW, Washington, DC 20375, USA*

In 1995, an expedition on board the research vessel FS *Polarstern* explored the impact site of the Eltanin asteroid in the Southern Ocean, the only known asteroid impact into a deep ocean basin. Analyses of the geological record of the impact region place the event in the late Pliocene (~2.15 Myr) and constrain the size of the asteroid to be >1 km. The explosive force inferred for this event places it at the threshold of impacts believed to have global consequences, and its study should therefore provide a baseline for the reconstruction and modelling of similar events, which are common on geological timescales.

Of the ~140 known terrestrial impacts[1], the late Pliocene impact of the Eltanin asteroid into the Bellingshausen Sea (eastern Pacific sector of the Southern Ocean) is the only example of an impact on the 60% of the Earth's surface covered by deep ocean basins. Evidence of this impact was first discovered as an iridium (Ir) anomaly in 1981 (ref. 2) in a sediment core collected in the mid-1960s by the USNS *Eltanin*. Subsequent studies[3] showed that meteoritic ejecta are present in three sediment cores separated by 500 km and that the Ir is largely concentrated in vesicular debris that formed by melting of the asteroid as it impacted the ocean. The ejecta contain meteorite fragments of a basaltic achondrite[4] that have been named the Eltanin meteorite (an anomalous mesosiderite), and rare spherules containing Ni-rich magnesioferrite spinel[5], a component also found in Cretaceous/Tertiary (K/T) boundary ejecta[6].

Here we present the results of a more comprehensive exploration of the Eltanin impact area, combining bathymetric, seismic and marine-geological studies, accomplished during the 1995 expedition ANT-XII/4 of the FS *Polarstern*. The surveyed area is in the vicinity of the location of Eltanin Core E13-4 (57° 47.2′ S, 90° 47.6′ W, 4,700 m depth), where the highest concentrations of impact debris were encountered[3]. We found evidence of erosion and redeposition of sediments of various ages covering a time span of 50 Myr. We describe an allochthonous impact-related sedimentary succession resting with erosional contact on autochthonous pre-impact sediments. This documents the impact-triggered resuspension and mass transport of sediments from the sea floor and the subsequent decrease in turbulent energy during redeposition of this reworked material. The lower part of the sequence is made up of a 'chaotic', unsorted intrabasinal breccia that includes sediment clasts of different sizes, lithologies and ages overlain by a laminated and graded foraminiferal sand. The uppermost part of the sequence consists of biogenic oozes of various ages that were sedimented from a cloud of sediment dispersed in the water column. Meteoritic ejecta, which were probably airborne and settled through the 5 km water column, began to accumulate on the ocean floor 4 hours after the impact. The impact might be responsible for producing a seismically transparent sediment layer, typically 20–40 m thick and extending hundreds of kilometres across the ocean floor. Although there is evidence for disturbance and removal of large volumes of sediments our survey did not find evidence that a crater was excavated on the ocean floor.

We estimate that the size of the impacting asteroid was in the range of 1–4 km with an explosive force in the range of 10^5–10^7 Mt TNT explosive. Although an impact of this size would have excavated a 15–40-km diameter crater on a continent[7] it is unlikely to penetrate the crust of the deep-ocean basins. In contrast to continental impacts, the Eltanin impact might have caused devastating megatsunamis along many coastlines and might have had an effect on the climate by the ejection of large volumes of water and salts that would be deposited in the upper atmosphere. The ~2.15-Myr age of the impact precedes a period of intensified cooling. Curious phenomena reported for the Pliocene might be related to this impact, including unusual bonebeds in Peru, marine Pliocene sediments covering coastal Antarctic areas, and marine microfossils in the Transantarctic Mountains.

Survey in the impact region

The survey area is on the Pacific–Aluk portion of the Antarctic plate[8], where basement ages are ~60 Myr (Fig. 1a). Topography mapped by Hydrosweep swath-bathymetry revealed an irregular seamount system, the San Martin seamounts, with minimum water depths of ~2,500 m. The surrounding rugged deep-sea floor has depths of ~5,000 m (Fig. 1b).

In the abyssal portions of the survey area, a high-resolution seismic survey with a Parasound echosounding system revealed a sequence of well-stratified reflectors typically 20–30 m thick, underlain by a seismically transparent zone. The base of the Eltanin–Polarstern Transparent Zone (EPTZ) is a strong reflector, which prevents deeper penetration of the acoustic signals in most areas. In some places, such as north of the seamount, the EPTZ increases to more than 60 m, filling in an irregular topographic structure, where

the strong reflector probably marks basement (Fig. 2). In the areas east of the seamounts the EPTZ displays a more uniform thickness ranging between 20 and 40 m, following the bottom topography. The EPTZ was not discerned on the seamounts, where rough topography disturbed the echosounding signal. Seismically transparent layers can represent sequences of stratified sediments with almost zero acoustic impedance contrasts at their layer boundaries or a zone of chaotically deposited sedimentary material. Thus the EPTZ was suspected to be related to deposits disturbed by the impact.

At most localities, the EPTZ was beyond the reach of our 20-m-long piston coring device because of the greater thickness of the overlying acoustically stratified sequence. However, we successfully penetrated the EPTZ at eight localities where we observed that the seismically stratified sediments and the EPTZ are thinning towards the edges of topographic highs and hence we were able to recover impact deposits. Three cores with complete sections provide a depth profile from Core PS2709-1 near the top of the seamount (57° 46.8′ S, 90° 59.9′ W; 2,707 m depth), to PS2708-1 at intermediate water depths (57° 35.4′ S, 91° 13.2′ W; 3,965 m), and to PS2704-1 in the abyssal basin north of the seamount (57° 23.4′ S, 90° 48.4′ W; 4,961 m; Fig. 1b). In two cores (PS2714-1, PS2705-1) we recovered only the uppermost portion of the impact deposit and in three others (PS2702-1, PS2706-1, PS2710-1), significant parts of the section seem to be missing because of an erosional event that affected sediments around the seamounts in the early Pleistocene.

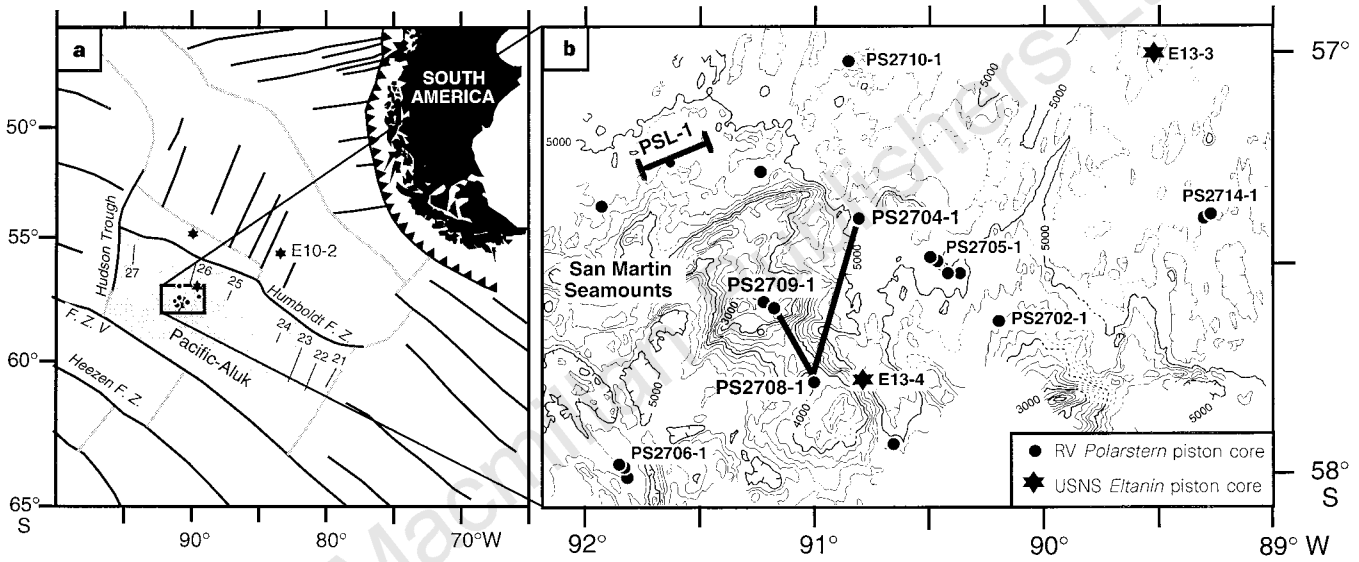

Figure 1 Schematic representation of the Bellingshausen Sea tectonic setting showing major fracture and subduction zones; the Pacific–Aluk portion of the Antarctic plate is shaded and shows magnetic lineations in accordance with ref. 8 (**a**). Box on Pacific–Aluk indicates area with extensive bathymetric, seismic and sediment coring survey in the vicinity of San Martin seamounts (**b**). Bathymetric map (200-m contour interval) of area affected by the asteroid impact shows the location of core transect PS2709-1–PS2704-1 (Fig. 3), and other Polarstern and Eltanin cores discussed in the text. PSL-1 indicates the location of the Parasound echosounding profile in Fig. 2.

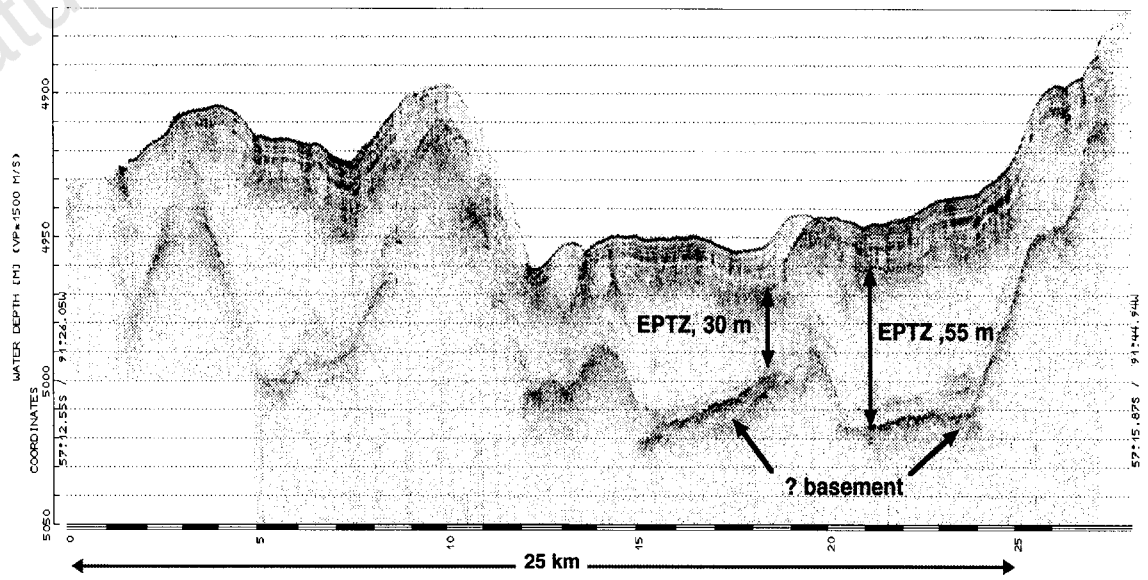

Figure 2 Parasound echosounding of the sediments along the transect PSL-1 to the north of the seamounts (Fig. 1b). Up to 60 m of seismically transparent sediments, representing the Eltanin–Polarstern Transparent Zone (EPTZ) underlie the well-stratified late Pliocene to recent sediments and fill a rough topography that might be basement. The EPTZ might be largely sediments ripped up and redeposited by the impact. The Parasound system typically allows seismic penetration of the upper 100–300 m of sediment.

We recognize five sedimentary units (SU). The lowermost SU V consists of autochthonous, undisturbed sediments. In PS2708-1 the lowermost 163 cm are SU V consisting of a calcareous nannofossil ooze assigned to the middle Eocene (NP16, ~43–41 Myr) (Fig. 3). The clays in the ooze bear >90% well-crystallized smectite, with associated clinoptilolite and goethite. In PS2704-1, a homogeneous sequence of clay (~80% smectite) with frequently changing magnetic polarities at mostly steep inclinations occurs below 1,411 cm. However, traces of diatoms with a first occurrence datum in the late Pliocene predating the impact event (*Fragilariopsis kerguelensis*) cause us to suspect that this sequence might be partly disturbed and more appropriately belongs in SU IV, except the section below 1,733 cm, where clays are almost pure smectite (99%) like that in the Eocene section of PS2708-1 (Fig. 4).

The impact-related deposit begins with SU IV, an allochthonous, chaotic mixture of sedimentary clasts as large as 50 cm, with different lithologies and ages (Figs 3, 5a). At the top of the seamount (PS2709-1) SU IV is composed of clasts of middle Eocene to Oligocene, middle Miocene and Pliocene calcareous nannofossil and foraminiferal oozes (~90% $CaCO_3$) with minor admixtures of Pliocene diatoms and radiolarians (Fig. 4). In PS2708-1, SU IV contains manganese nodules, and a fragment of a ~15-cm-thick manganese crust interbedded with soft sediment clasts of barren clays, middle Eocene calcareous muds and Pliocene diatom oozes and muds. In PS2704-1 SU IV has two distinct subunits (Fig. 3). The lower, SU IVB, contains sediment clasts up to 15 cm in diameter that are composed of clays with only traces of poorly preserved diatoms, probably Pliocene in age. SU IVA is characterized by smaller clasts (0.5–2 cm) embedded in a sandy matrix and contains up to 40% carbonate composed of Eocene to Oligocene foraminifera and nannofossils besides rare diatoms that range in age around the Oligocene/Miocene boundary, in the middle–late Miocene and the Pliocene.

SU III is a laminated, well-sorted and graded sand (Figs 3, 5b). In PS2709-1 it consists predominantly of Pliocene foraminifera with admixed Palaeogene and Miocene calcareous nannofossils. In PS2708-1 and PS2704-1, SU III is a mixture of biosiliceous and calcareous sediments including Palaeogene and Neogene microfossils (Fig. 4), as well as a few basaltic rock fragments (PS2704-1).

SU II consists mainly of fine-grained sediment (Fig. 3). Whereas in PS2708-1 this unit is ~115 cm thick and unbioturbated, in PS2709-1 and PS2704-1 it is much thinner and significantly disturbed by bioturbation. In the shallow sites (PS2709-1, PS2708-1) above the carbonate compensation depth (CCD) SU II is characterized by the occurrence of displaced Palaeogene calcareous microfossils, mainly Eocene in age (Figs 4, 6). The deep PS2704-1 contains reworked Neogene and Oligocene diatoms and clinoptilolite, most probably originating from Palaeogene clays (Fig. 4).

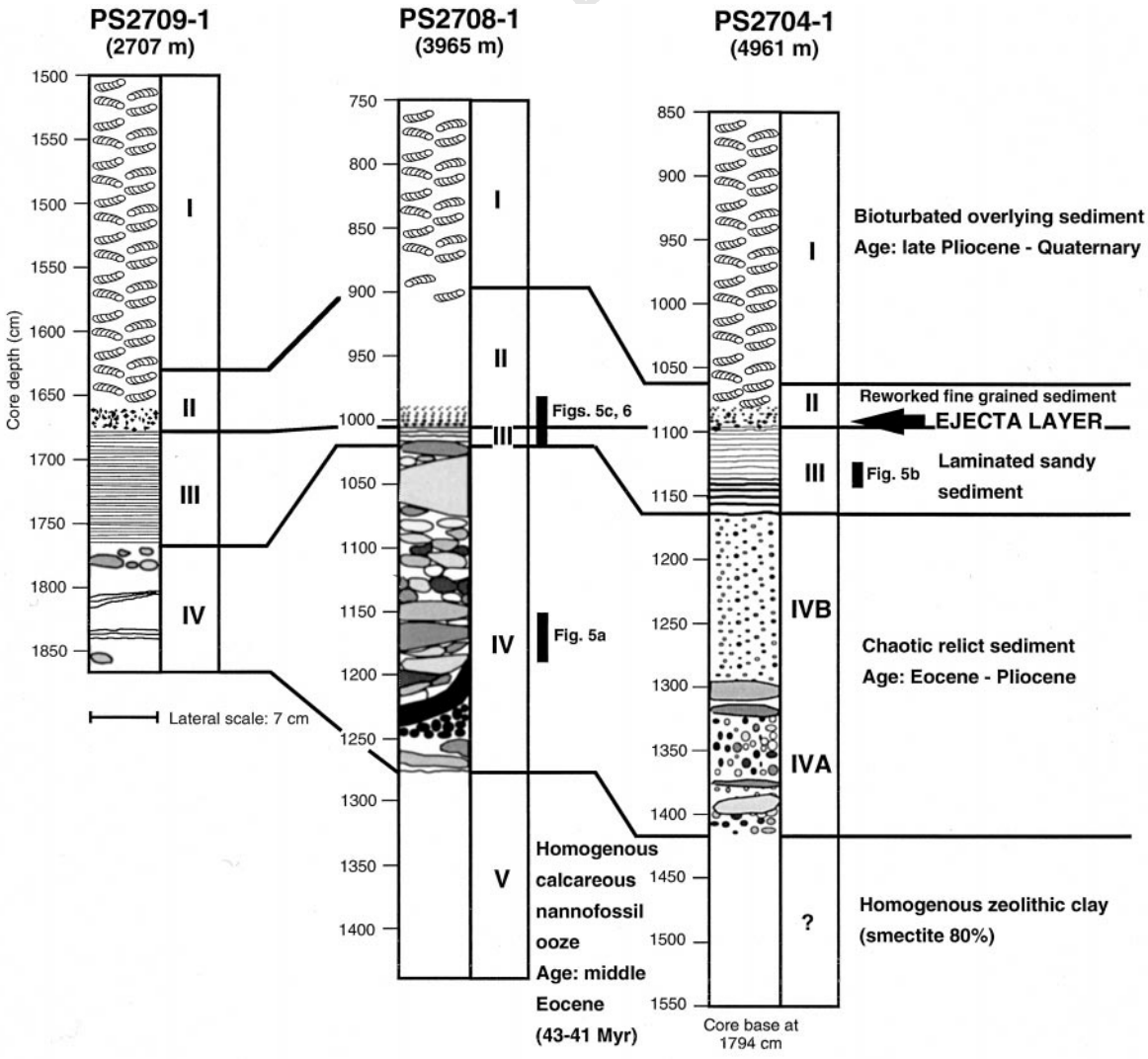

Figure 3 Piston cores PS-27091-1, PS2708-1 and PS2704-1 provide a depth transect from the top of the San Martin seamounts to the abyssal floor in the north (Fig. 1b). Five sedimentary units are recognized. SU II, III, and IV were deposited in the brief interval after the impact. Core logs include information on sediment structure only.

Meteoritic ejecta were found within the uppermost portion of SU III and throughout SU II. Maximum concentrations making up to 20% of the total sediment occur in the lowermost 10–20 cm of the ejecta-bearing interval. The meteoritic particles reveal an upward decrease in grain size overprinting the grain size distribution of the non-meteoritic material (Fig. 6). The ejecta consist mainly of vesicular impact melt, but few per cent of the ejecta are unmelted meteorite fragments, and trace amounts of spinel-bearing spherules have been observed. We have separated 7.9 g of coarse impact debris. Of this, 0.42 g are unmelted meteorite particles, making the

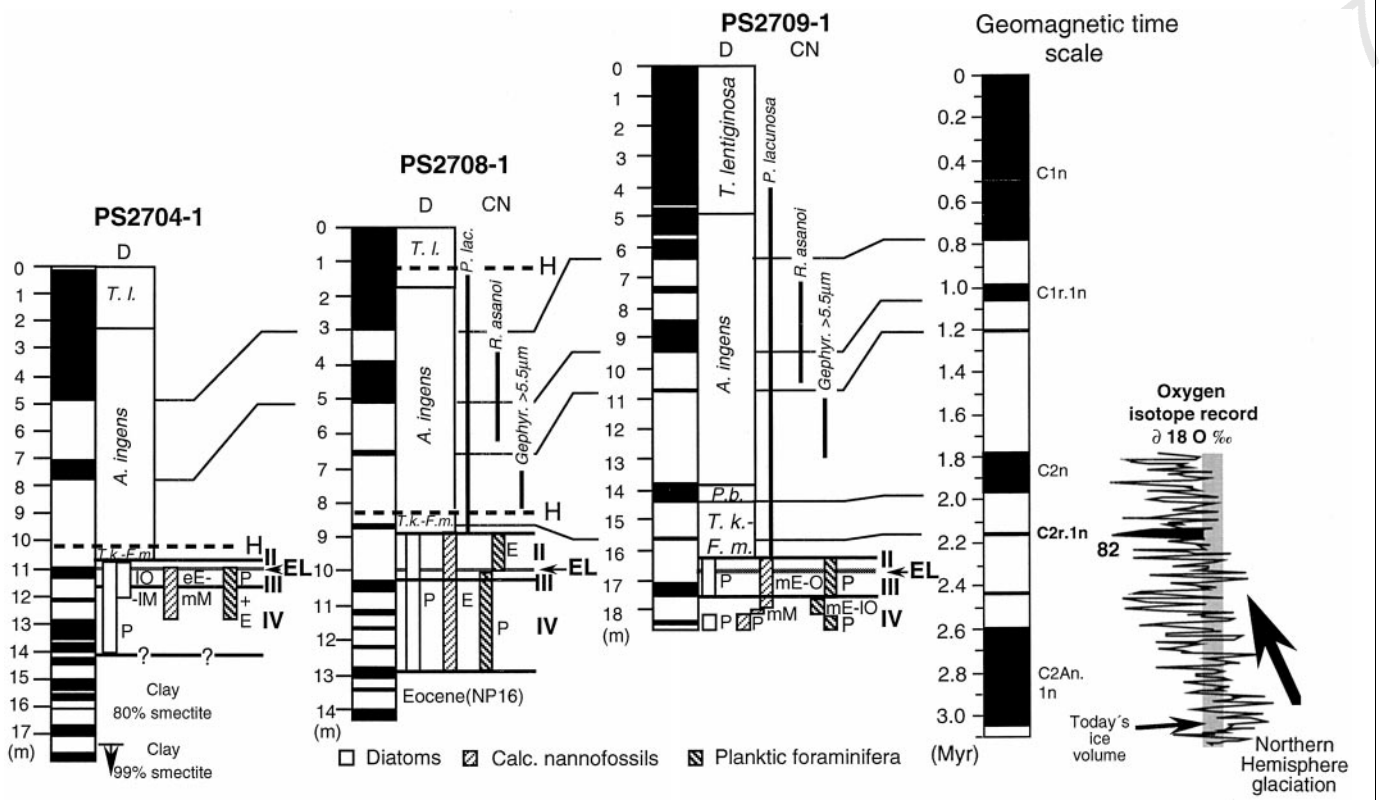

Figure 4 Age determination of the impact event and reworked impact deposits based on combined magnetostratigraphy and biostratigraphy of PS2704-1, PS2708-1 and PS2709-1. Impact-related SU IV, III and II and ejecta layer (EL) are marked. The youngest impact-related SU II is close to the Réunion geomagnetic event (C2r.1n). The impact event thus closely predates C2r.1n, and is close to isotope glacial event 82 (ref. 32). Bars on the impact-related interval indicate the schematically stratigraphic ages of diatoms, calcareous nannofossils and planktic foraminifera predominantly recovered in SU IV, III and II (eE, early Eocene; mE, middle Eocene; IO, late Oligocene; mM, middle Miocene; IM, late Miocene; P, Pliocene). Latest Pliocene to early Pleistocene sediments are omitted by a hiatus (H) in PS2704-1 and PS2708-1. Magnetic data are correlated with the standard geomagnetic polarity timescale[10]. Stable characteristic remnant magnetization directions were determined from detailed alternating field demagnetization up to 80 mT strength. Polarities were determined directly from the sign of the steep inclinations. Biostratigraphy by diatom (D) zonation[9] (zonal names: *T. l.*, *Thalassiosira lentiginosa*; *P. b.*, *Proboscia barboi*; *T. k-F. m.*, *Thalassiosira kolbei–Fragilariopsis matuyamae*) and calcareous nannofossil (CN) ranges[12,33] and zonation[34]. Determination of Eocene NP16 Zone (PS2708-1) is based on the presence of taxa such as *Reticulofenestra umbilica* and *Chiasmolithus solitus* and dated following ref. 35.

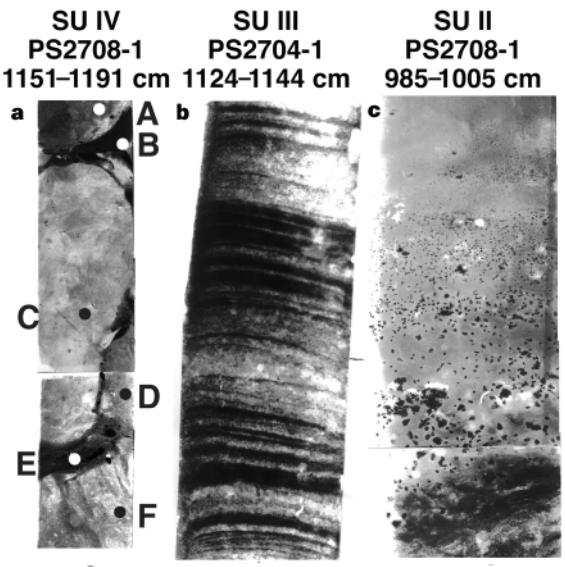

Figure 5 Details of the three sedimentary units formed by the impact illustrated by X-ray radiographs (compare Fig. 3). **a**, SU IV contains ripped up sediment clasts. In the section illustrated, six distinct sediments can be distinguished (A, diatom mud, age ~late Gauss Chron; B, calcareous nannofossil ooze, age ~mid-Eocene; C, diatom ooze, age ~mid-Pliocene; D, diatom mud, age early late Pliocene; E, mixed calcareous Eocene biosiliceous Pliocene; F, diatom ooze, age ~time of impact). **b**, SU III is a laminated sand. In PS2704-1, where it is best developed, it contains carbonates (30–60%) that must have been transported from the seamount ~40 km away. Interval 1,124–1,144 cm contains Palaeogene (~80%) and Pliocene (~20%) planktic foraminifera and late Oligocene–mid-Miocene and Pliocene diatoms. **c**, SU II contains fine-grained sediments that settled from a cloud in the water column consisting of Eocene calcareous nannofossils and foraminifera (Fig. 6) and predominantly mid-Pliocene diatoms. Graded meteorite ejecta can be seen as coarse grains starting at the boundary between SU III and SU II in PS2708-1 at ~1,003 cm depth. Note that the section for SU IV (**a**) is at 50% of the scale for the other two.

unmelted fraction of the meteoritic ejecta 5%. Most of the ejecta mass is in particles from 0.5 to 5 mm in size. The largest pieces have been found in the top of SU III in PS2704-1, including an unmelted meteorite 1.5 cm in length at 1,097 cm, and a 9 mm vesicular particle at 1,096 cm. Although stratification is not evident in the host sediment of SU II, the ejecta are concentrated at different layers in PS2708-1, where the lack of bioturbation allowed the best preservation of the fallout interval (Fig. 5c). This layering is seen to influence Ir and chromium (Cr) concentrations (Fig. 6). Similar, but less well-defined, layering is also present at PS2704-1.

Overlying the impact deposits, SU I is an undisturbed and bioturbated sequence of late Pliocene to Quaternary biogenic sediments.

Analyses of combined magnetostratigraphic and biostratigraphic data, including diatom and calcareous nannofossil stratigraphies, place the base of SU I, and thus the impact age, into the *Thalassiosira kolbei–Fragilariopsis matuyamae* diatom zone[9] directly below the magnetostratigraphic Réunion Event (C2r.1n). This event is in the lower Matuyama Chron and has been assigned an age of 2.15–2.14 Myr (ref. 10) (Fig. 4). Whereas in PS2709-1 SU I has been deposited continuously at sedimentation rates of 0.5–0.9 cm kyr^{-1}, the sediment sequences in PS2708-1 and PS2704-1 are disturbed by a hiatus that omits part of the middle Matuyama Chron (Fig. 4). The post-impact erosional event might be responsible for the lack of SU II and III, including meteorite ejecta, in such cores as PS2702-1, PS2706-1 and PS2710-1.

We resampled Eltanin cores E13-3, E13-4 and E10-2, all of which are known to contain ejecta[3]. These cores are in incomplete state and dried out 30 years after their collection. On the basis of available core descriptions[11] and our analyses we suggest that they include sediment sequences similar to those documented in the Polarstern cores. In E13-4, recovered close to the seamounts (Fig. 1b), sediments below the ejecta horizon (1,298 cm depth), formerly interpreted as a continuous Eocene deposit[12], seem to be the chaotic SU IV. The sediments are a mixture of barren zeolitic clays rich in well-crystallized smectite (>95%) and Eocene calcareous nannofossil ooze. We also got one sample at 1,305 cm that contains Pliocene diatoms stratigraphically below an early Eocene nannofossil ooze at 1,303 cm. In E13-3 and E10-2, ~100 km and 530 km to the northeast of the San Martin seamounts, respectively (Fig. 1), sediments below the ejecta might also be disturbed by the impact. This is indicated by trace occurrences of diatoms that range in age from *early* late Pliocene to Quaternary and also in the Miocene, intervals dominated by well-crystallized smectite (E10-2, 750–948 cm) and descriptions of sedimentary structures as 'lumps and blebs'[11].

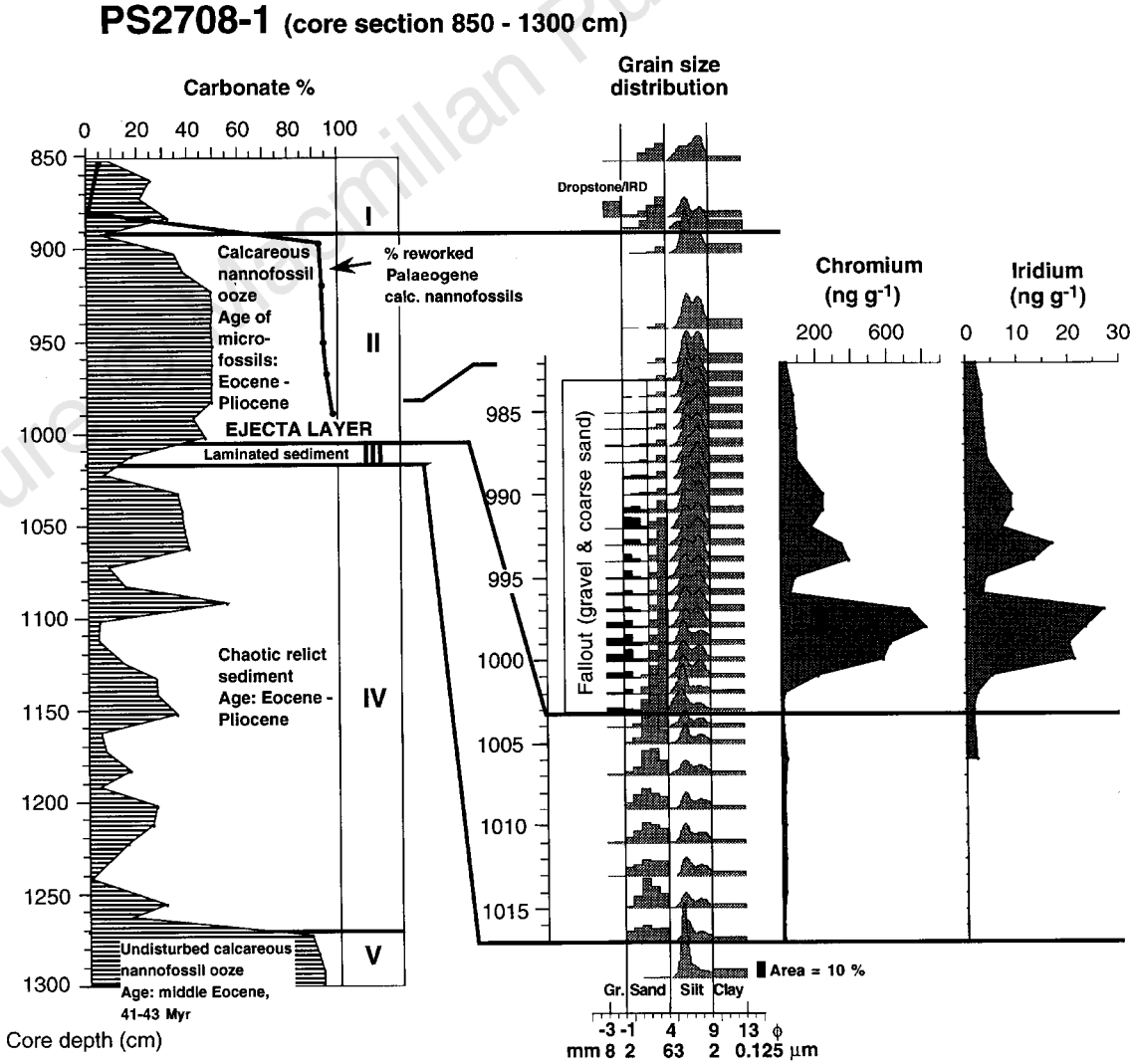

Figure 6 Core PS2708-1 carbonate content in impact-related sediment units, and grain size distribution in an expanded section of the laminated SU III and the ejecta-rich sediments of SU II (Fig. 3). Grain sizes show gradation of sand sizes in the laminated SU III. A sharp increase in gravel and coarse sand components is at 1,003 cm, where the ejecta debris is first observed at the base of SU II. Peaks in the measured concentrations of Cr and Ir coincide with the graded layers of high ejecta concentrations that can be observed in X-ray photographs (Fig. 5c).

Depositional model

We interpret our sediment cores as recording a sequence of processes involving sediment mass erosion and redeposition at decreasing energy level, accompanied by fallout of impact debris through air and water. These processes occurred over a period of at least several hours after the impact event. The impact ripped up and redeposited sediments on the San Martin seamounts and in the surrounding abyssal basin. Some of the displaced sediment has been redeposited rapidly as large fragments, commonly 10–50 cm in size on and in the vicinity of the seamounts (SU IV; Fig. 5a). This involved significant lateral and vertical transport, since fragments of clay-rich sediment typical of the abyssal basin were found above the CCD in PS2708-1, ~1 km above the present abyssal sea floor. In turn, carbonate-rich clasts and calcareous microfossils were deposited out in the basin below the CCD as recorded in PS2704-1, ~40 km northeast of the seamount crest.

The laminated sediments of SU III (Fig. 5b) were deposited from a turbid flow. The presence of SU III in the abyssal areas (PS2704-1) as well as on the top of the seamount (PS2709-1) indicates that there was both downslope gravitational sediment transport into the abyssal basin and rapid sedimentation of well-sorted sand-sized particles (for example, foraminifera) from sediments stirred up into higher levels of the water column. We can estimate the duration of this event in the abyssal basin, by using the settling velocity of the 1.5-cm meteorite (measured at 37 cm s^{-1}) recovered from the top of SU III at PS2704-1. On the assumption that this rock settled through the water column (~5,000 m) to reach the abyssal floor, deposition of SU III did not conclude at site PS2704-1 until 4 hours after the impact.

SU II records the settling of fine-grained particles through the water column including a cloud of resuspended bottom sediment, and meteoritic ejecta that were most probably airborne. Some of the non-meteoritic sediment might also be ejecta, but we lack criteria to distinguish this. The observation of concentrations of the meteoritic ejecta in different horizons, documented in X-ray radiographs (Fig. 5c) and Ir and Cr distributions in PS2708-1 (Fig. 6), indicates that currents were still active during the early phases of sedimentation of SU II. The transition from SU III to SU II might reflect a gradual transition to less turbulent conditions, rather than a boundary between two distinct events. Deposition of SU II probably lasted for several hours to days after the impact.

At sites further from the seamounts, our information is less detailed but there is evidence of disturbance over a broad region. At PS2714-2 (57° 22.7′ S, 89° 16.1′ W; 5,178 m depth; Fig. 1b), ~100 km east, we recovered sediment from the top of SU II showing a mixture of late and middle Pliocene diatoms. At the Eltanin cores, E13-3 and E10-2 mixed microfossil assemblages and clays have been identified below the impact ejecta, indicating that sediment disturbance and the sediment cloud extended at least 500 km to the east of the seamounts. The large areal extent of the EPTZ also indicates widespread disturbance. These acoustically transparent sediments are believed to be the chaotically disturbed unit SU IV. Because we recovered our cores where echosounding indicated that seismically stratified and transparent sediments were thinning, we did not recover the complete disturbed section and we assume that impact units SU II, III and IV in our cores are thinner than typical.

Multichannel seismic data from a west–east profile across the survey area show that in some areas of the abyssal basin sediments are 200–300 m thick, but near the seamounts there are regions where sediment cover is virtually absent. It is possible that the Eltanin impact ejected large volumes of sediment out of our survey area, and that all might remain is the larger rubble that fills in the exposed topography of the ocean crust.

We know that sediments as old as early Eocene (~50 Myr in E13-4, PS2704-1) were affected by the impact. In fact, early to late Eocene and middle Pliocene sediments are abundant in our samples from SU II–IV. Significant occurrences of diatoms ranging from late Oligocene to early Miocene (PS2704-1) and rarer findings of microfossils characteristic of the middle and late Miocene indicate that such sediments were also affected by the impact (Fig. 4). We know that Miocene sediments exist in the area because ~3 m of late-middle to late Miocene diatom oozes were recovered at PS2706-1 (57° 58.0′ S, 91° 51.5′ W), ~55 km south of the San Martin seamounts (Fig. 1b).

Sediment reworking is also evident from clay mineralogy. Clay mineral assemblages of the impact-related sediments show compositions intermediate between those characteristic of pre-Miocene altered sediments and younger sediments, indicating mixing of clay minerals from pre-impact strata of various ages. Clay mineral assemblages consisting of almost pure well-crystallized smectite in association with zeolites, as recorded in Eocene clays of PS2708-1 (SU V) and at the base of PS2704-1 (Fig. 4), are consistent with authigenic formation by submarine diagenesis (hydrothermal alteration) and are also known from other parts of the Bellingshausen Sea in sediments older than late Miocene[13], including Core PS2664-1 recovered ~400 km north of the San Martin seamounts. Sediments younger than the late Miocene differ markedly, consisting of smectite that is only moderately crystallized, and significant amounts of terrigenous illite and chlorite[13], as also recorded in the late Pliocene to Quaternary sequences of SU I.

Reconstructing the impact event

Previous estimates of the size of the Eltanin asteroid range from 0.5 to 2 km diameter[3]. The lower estimate was based on a model of the distribution of ejecta that we now find to be too conservative, as it neglected the possibility that a large fraction of the projectile might have been vaporized and distributed globally. High concentrations of ejecta were deposited throughout our survey area. Current estimates of ejecta deposited at sites PS2704-1, PS2708-1 and PS2709-1 are ~500, 830 and 670 mg cm^{-2}, respectively. These compare well with debris estimates of 790 and 187 mg cm^{-2} at E13-4 and E13-3, respectively[3]. Considering the large area of disturbance (including the deposition of displaced sediment as much as 500 km from the seamounts and the apparent ejection of large volumes of sediment) and the probability that most of the asteroid was ejected far from the impact region, we propose a more reasonable lower limit on the asteroid diameter of 1 km. The 2 km upper limit was constrained by models indicating that during an oceanic impact an asteroid would penetrate the water to depths several times its diameter[14]. The latter constraint was necessary because there is no evidence from the impact melt that the projectile mixed with silicate target material[4]. However, recent models indicate that the penetration of the asteroid (its stagnation depth) should be on the order of the projectile diameter[7], not several times greater. For typical impact angles of 45°, projectiles as large as 3 or 4 km should avoid mixing with the ocean crust. Thus the upper-limit estimate on the Eltanin asteroid should be revised to ~4 km.

At typical asteroid velocities (~20 km s^{-1}), projectiles in the size range of 1–4 km have explosive energies in the range of 10^5–10^7 Mt TNT. These energies are at the threshold of those considered necessary to cause global devastation[15,16]. All impactors in this range will generate devastating megatsunamis. At 1 km the Eltanin asteroid would have generated tsunamis on the order of 20–40 m over deep water approaching South America and Antarctica, which might have reached runup heights on the continental margins 10–25 times higher[17]. Deep-water waves 5–10 m high would have extended into the North Pacific and around the Southern Ocean. Evidence of these megatsunamis should be present in sediments throughout the Pacific and Southern Ocean shores. We note geological anomalies that could be related. On the Peruvian coast, near Pisco, an unusual and unexplained mixture of complete marine and terrestrial mammal skeletons was found in coastal marine sediments that could be late Pliocene in age[18]. In coastal east Antarctica (Larseman Hills, Windmill Island, Indian sector)

late Pliocene deposits consisting of marine diatomaceous shallow water sediments and only a few decimetres thick are located several tens of metres above recent sea level[19]. These are probably allochthonous and might have been caused by up-shore transport of shelf sediments by a tsunami.

The Eltanin impact was certainly large enough for global distribution of ballistic ejecta[16]. The ejecta would consist mainly of water from the oceanic target, but would include significant amounts of asteroidal material, salts and probably marine sediments. Deposition of water and salts into the upper atmosphere, and formation of NO caused by the ionization of atmospheric nitrogen, have been hypothesized to have the potential to affect insolation for periods of years, and possibly even to deplete the ozone layer[16]. The actual extents of these effects are all model dependent and thus poorly constrained. They cannot be specifically examined in our cores. However, we note that the revised age of 2.15 Myr places the impact close to marine oxygen-isotope stage 82. This time is significantly after the establishment of Northern Hemisphere ice sheets, but close to one of the strongest cooling events in this time period (Fig. 4). The age of the Eltanin impact is not marked by disturbances (extinctions) in the marine microfossil record, but a transient depletion of the ozone layer might have had an effect on terrestrial life.

The silicate fraction of the ejecta would be difficult, but not impossible, to detect at sites distant from the impact. Globally distributed meteoritic ejecta could amount to 0.4–25 mg cm^{-2} for 1–4-km asteroids, respectively. Corresponding Ir anomalies of 0.1 ng cm^{-2} for a 1-km asteroid might be undetectable, but the 6.4 ng cm^{-2} of a 4-km asteroid should be measurable. If only a small fraction of the ejecta ($\sim$0.05 km^3) was sediment, this would be sufficient to coat the surface of the Earth with traces of microfossils equivalent to a few diatoms per cm^2. Under most circumstances, we would expect such a deposit to be undetectable as these microfossils would be subject to dissolution and/or dilution by other biogenic components. Exceptions could be high-accumulation laminated sediments in the marine and lacustrine record. Other potential sites for preservation and detection of Eltanin ejecta are in the ice-free Transantarctic Mountains (TAM). These areas have been described as a cold-desert environment and thus have not been affected by strong weathering or disturbances by ice and water run-off since at least 3.8 Myr (refs 20, 21). Interestingly, rare occurrences of marine diatoms, minor quantities of radiolarians and calcareous nannofossils, and small marine sediment fragments with stratigraphic ages ranging between the Eocene and the late Pliocene have been reported from glaciogenic sediments of the TAM known as the Sirius Group deposits. But these findings were interpreted to indicate that drawdown of the East Antarctic Ice Sheet (EAIS) during the Late Pliocene led to flooding of intracratonic Antarctic basins and that the subsequent glacial advance excavated and transported the microfossils to the TAM[22,23]. This hypothesis of unstable mid-Pliocene ice volumes has been widely debated[24–26], as it would require significant warming at high latitudes not observed in other studies[27] and it raises questions about the stability of the modern ice sheet. To resolve the Sirius enigma it was proposed that the microfossils have been imported by aeolian transport. Aeolian transport provides a viable mechanism for explaining the occurrence of freshwater[28,29], non-Antarctic marine[29] and modern Antarctic[29,30] marine diatoms, reported on the Antarctic ice and terranes. However, the occurrence of extinct Cenozoic diatoms and other microfossils, as well as sediment fragments, that must have originated in deep-sea Southern Ocean sediments has not yet been adequately explained by the aeolian transport mechanism[31]. We suggest that an elegant solution might be that the introduction of marine microfossils and sediment was as ejecta from the Eltanin impact. This mechanism is distinct from aeolian import in that the ejecta are derived from a point source and transported above the atmosphere. A possible impact source is supported by the fact that the Sirius microfossils fit well within the age of sediments disturbed by the impact, including upper Eocene, upper Oligocene/lower Miocene, and middle to lowermost Pliocene taxa. Many of the taxa reported in the Sirius Group till[22] were found in SU III and II. The youngest diatoms, used for dating the hypothetical mid-Pliocene EAIS deglaciation (*Thalassiosira vulnifica*, *T. kolbei*), were present in surface sediments when the Eltanin impact occurred. Further research into this impact, and also into the distribution pattern and the quantity of microfossils in the TAM deposits, will test the viability of this transport mechanism. □

Received 21 January; accepted 30 September 1997.

1. Grieve, R. A. F. & Shoemaker, E. M. in *Hazards Due to Comets and Asteroids* (ed. Gehrels, T.) 417–462 (Univ. Arizona Press, 1994).
2. Kyte, F. T., Zhou, Z. & Wasson, J. T. High noble metal concentrations in a late Pliocene sediment. *Nature* **292,** 417–420 (1981).
3. Kyte, F. T., Zhou, L. & Wasson, J. T. New evidence on the size and possible effects of a late Pliocene oceanic impact. *Science* **241,** 63–65 (1988).
4. Kyte, F. T. & Brownlee, D. E. Unmelted meteoritic debris in the Late Pliocene Ir anomaly: evidence for the impact of a nonchrondritic asteroid. *Geochim. Cosmochim. Acta* **49,** 1095–1108 (1985).
5. Margolis, S. V., Claeys, P. & Kyte, F. T. Microtektites, microkrystites and spinels from a late Pliocene asteroid impact in the Southern Ocean. *Science* **251,** 1594–1597 (1990).
6. Kyte, F. T. & Smit, J. Regional variation in spinel compositions: an important key to the Cretaceous–Tertiary event. *Geology* **14,** 485–487 (1986).
7. Melosh, H. J. *Impact Cratering* (Oxford Univ. Press, New York, 1989).
8. Cande, S. C., Herron, E. M. & Hall, B. R. The early Cenozoic history of the southeast Pacific. *Earth Planet. Sci. Lett.* **57,** 63–74 (1982).
9. Gersonde, R. & Barcena, M. A. Revision of the upper Pliocene–Pleistocene diatom biostratigraphy for the northern belt of the Southern Ocean. *Micropaleontology* (in the press).
10. Cande, S. C. & Kent, D. V. J. Revised calibration of the geomagnetic polarity timescale for the Late Cretaceous and Cenozoic. *Geophys. Res.* **100**(B4), 6093–6095 (1995).
11. Anonymous. Marine Geology USNS Eltanin Cruses 9–15, core description and locations. (Contr. 11, Sedimentology Research Laboratory, Dept. of Geology, Florida State Univ., 1965).
12. Wei, W. Calibration of upper Eocene–lower Pleistocene nannofossil events with oxygen isotope stratigraphy. *Paleoceanography* **8,** 85–99 (1992).
13. Gorbunova, Z. N. Clay-size minerals from cores of the southeast Pacific Ocean. *Init. Rep. DSDP* **35,** 479–488 (1976).
14. O'Keefe, J. D. & Ahrens, T. Impact mechanics of the Cretaceous–Tertiary extinction bolide. *J. Lunar Planet. Sci.* **12,** 785–787 (1981).
15. Chapman, C. R. & Morrison, D. Impacts on the Earth by asteroids and comets: assessing the hazard. *Nature* **367,** 33–40 (1994).
16. Toon, O. B., Zahnie, K., Morrison, D., Turco, R. P. & Covey, C. Environmental perturbances caused by the impacts of asteroids and comets. *Rev. Geophys.* **35,** 41–78 (1997).
17. Hills, J. G., Nemchinov, I. V., Popov, S. P. & Teterev, A. V. in *Hazards Due to Comets and Asteroids* (ed. Gehrels, T.) 779–789 (Univ. Arizona Press, 1994).
18. Muizon, C. de. Les vertébrés fossiles de la formation Pisco (Pérou). 1: Deux nouveaux *Monochinae* (Phocidae, Mammalia) du Pliocène de Sud-Sacaco. (Inst. Francais d'études Andines, Édit. recherche sur les Civilisations, Mémoire 6, Paris, 1981).
19. Quilty, P. G. in *Recent Progress in Antarctic Earth Science* (ed. Yoshida, Y.) 699–705 (Terra Scientific, Tokyo, 1992).
20. Hall, B. L., Denton, G. H., Lux, D. R. & Schlüchter, C. Pliocene paleoenvironment and Antarctic ice sheet behavior: evidence from Wright Valley. *J. Geol.* **105,** 285–294 (1997).
21. Bruno, L. A., Baur, H., Graf, T., Schlüchter, C., Signer, P. & Wieler, R. Dating of Sirius Group tillites in the Antarctic Dry Valleys with cosmogenic ^{3}He and ^{21}Ne. *Earth Planet. Sci. Lett.* **147,** 37–54 (1997).
22. Harwood, D. M. Diatoms from the Sirius Formation, Transantarctic Mountains. *Antarctic J.* **18,** 98–100 (1983).
23. Webb, P.-N., Harwood, D. M., McKelvey, B. C., Mercer, J. H. & Stott, L. D. Cenozoic marine sedimentation and ice volume variation on the east Antarctic craton. *Geology* **12,** 287–291 (1984).
24. Webb, P.-N. & Harwood, D. M. Late Cenozoic glacial history of the Ross Embayment, Antarctica. *Quat. Sci. Rev.* **10,** 215–223 (1991).
25. Barrett, P. J., Adams, C. J., McIntosh, W. C., Swisher, C. C. III & Wilson, G. S. Geochronological evidence supporting Antarctic deglaciation three million years ago. *Nature* **359,** 816–818 (1992).
26. Sugden, D. E., Marchant, D. R., Potter, N. Jr, Souchez, R. A., Denton, G. H., Swisher, C. C. III & Tison, J.-L. Preservation of Miocene glacier ice in east Antarctica. *Nature* **376,** 412–414 (1995).
27. Kennett, J. P. & Hodell, D. A. Evidence for relative climatic stability on Antarctica during the early Pliocene: a marine perspective. *Geograf. Ann.* **75,** 205–220 (1993).
28. Kellogg, D. E. & Kellogg, T. B. Non-marine diatoms in the Sirius Formation. *Antarctic J.* **19,** 44–45 (1984).
29. Barrett, P. J., Bleakly, N. L., Dickinson, W. W., Hannah, M. J. & Harper, M. A. Distribution of siliceous microfossils on Mount Feather, Antarctica, and the age of the Sirius Group. *Proc. Terra Antarctica* **3,** (in the press).
30. Burckle, L. H. & Potter, N. Jr. Pliocene–Pleistocene diatoms in Paleozoic and Mesozoic sedimentary and igneous rocks from Antarctica: a Sirius problem solved. *Geology* **24,** 235–238 (1996).
31. Stroeven, A. P., Pentrice, M. L. & Kleman, J. On marine microfossil transport and pathways in Antarctica during the late Neogene: evidence from the Sirius Group at Mount Fleming. *Geology* **24,** 727–730 (1996).
32. Shackleton, N. J., Hall, M. A. & Pate, D. Pliocene stable isotope stratigraphy of Site 846. *Proc. ODP Sci. Res.* **138,** 337–355 (1995).
33. Raffi, I., Backman, J., Rio, ,D. & Shackleton, N. J. Plio-Pleistocene nannofossil biostratigraphy and calibration to oxygen isotope stratigraphies from Deep Sea Drilling Project Site 607 and Ocean Drilling Program Site 677. *Paleoceanography* **8,** 387–408 (1993).
34. Perch-Nielsen, K. in *Plankton Stratigraphy* Vol. 1 (eds Bolli, H. B., Saunders, J. B. & Perch-Nielsen, K.) 427–554 (Cambridge Univ. Press, 1985).
35. Berggren, W. A., Kent, D. V., Swisher, C. C. III & Aubry, M.-P. in *Geochronology Timescales and Global Stratigraphic Correlation* (eds Berggren, W. A., Kent, D. V., Aubry, M.-P. & Hardenbol, J.) 129–212 (Spec. Publ. 54, Soc. of Economic Paleontologists and Mineralogists, 1995).

Acknowledgements. This research was supported by Acciones Integradas grants to R.G. and J.A.F., and an NSF grant to F.T.K. and J.A.B. We thank the crew of RV *Polarstern* for their substantial support.

Correspondence and requests for materials should be addressed to R.G. (e-mail: rgersonde@awi-bremerhaven.de).